

Fluctuation-Response Design Rules for Nonequilibrium Flows

Ying-Jen Yang*

Laufer Center of Physical and Quantitative Biology, Stony Brook University

Ken A. Dill

Laufer Center of Physical and Quantitative Biology, Stony Brook University

Department of Physics, Stony Brook University and

Department of Chemistry, Stony Brook University

Biological machines like molecular motors and enzymes operate in dynamic cycles representable as stochastic flows on networks. Current stochastic dynamics describes such flows on fixed networks. Here, we develop a scalable approach to *network design* in which local transition rates can be systematically varied to achieve global dynamical objectives. It is based on the fluctuation-response duality in the recent Caliber Force Theory—a path-entropy variational formalism for nonequilibria. This approach scales efficiently with network complexity and gives new insights, for example revealing the transition from timing- to branching-dominated fluctuations in a kinesin motor model.

Introduction: Consider a stochastic dynamical process transitioning among a network of states. In biophysics alone, such stochastic network flows are involved in the molecular mechanisms of motors and pumps [1–3], ultrasensitive switches in flagella [4, 5], the catalytic and allosteric actions in enzymes [6–9], phosphorylation cycles [10, 11], energy and chemical transduction [12, 13] and others. A fundamental goal is to control the long-term statistics of flows, given the local transition rates.

While Markov State Models and Master Equations describe these dynamics [14], they do not prescribe design. What is missing are principles for the optimization, control, and evolution of network flows: how should one systematically tune local transition rates to achieve specific global functions? Mathematically, this requires solving the response gradient—knowing exactly how local perturbations shift the long-term stochastic dynamics. However, raw gradients evaluated case-by-case do not reveal general principles. To navigate systematically, we exploit a key physical connection: general response relations are encoded in the system’s fluctuations.

Echoing Onsager’s regression hypothesis, recent nonequilibrium (NEQ) advances have established diverse fluctuation-response relations—equalities [15–20] or bounds [17, 20–23]—revealing that “noisier” mechanisms are inherently more susceptible to perturbative control. However, operationalizing this for NEQ flow design has some obstacles. First, design demands gradients, not just bounds. While performance limits are insightful [17, 20–23], inequalities inherently lack the local directional information needed to navigate parameter space. Second, we need to design and control the flux statistics too, not just the average state occupancy or the mean fluxes. Response relations on state occupancy [15, 22] do not control flux fluctuations. Third, scalability is paramount. Standard techniques, such as differentiating generating functions [24, 25] or summing over spanning trees [12, 14, 17, 21], offer physical insights but scale unfavorably with system size, rendering large-network

optimization computationally demanding. We need an actionable, complete and scalable framework.

Here, we address this need by establishing a principle-based design framework rooted in Caliber Force Theory (CFT) [26]. By projecting the independent transition noise [19] onto the orthogonal counting observables in CFT, we show that kinetic fluctuation-response relations originate from the theory’s fundamental observable-force conjugacy. This structure is encoded in a Jacobian matrix linking transition rates to *forces*. This underpinning provides a systematic and scalable design framework. Applied to a data-fitted kinesin model [2], it parses fluctuations to reveal the chemo-mechanical covariances underlying a load-dependent noise transition. Computationally, our framework overcomes the scalability bottleneck in evaluating gradients for the means and variances of fluxes in large networks. Analytically, it unifies NEQ response relations, extending previous results [17, 18, 20] and deriving kinetic bounds reflecting population depletion and Le Chatelier-like compensation. This framework transforms the geometry of spontaneous fluctuations into a scalable “road-map” for gradient-based design.

Theoretical Framework: Our foundation here is CFT, a dynamical variational formalism that mirrors the structure of equilibrium (EQ) thermodynamics [26]. We begin by considering the *path entropy* of Markov jump processes—defined as the logarithm of path probability ratio $\ln(\mathcal{P}_{\mathbf{k}}/\mathcal{P}_{\mathbf{u}})$. It measures the path-wise entropic cost of driving a unit-rate reference process \mathbf{u} to the dynamics with transition rate \mathbf{k} . For a path ω_t with duration t , it can be expressed in terms of *extensive counting observables* [27]:

$$\ln \frac{\mathcal{P}_{\mathbf{k}}(\omega_t)}{\mathcal{P}_{\mathbf{u}}(\omega_t)} = \sum_{i \neq j} N_{ij}(\omega_t) \ln k_{ij} - \sum_i T_i(\omega_t) \varepsilon_i(\mathbf{k}), \quad (1)$$

where N_{ij} is the number of transitions $i \rightarrow j$, T_i is the total dwell time of state i , and $\varepsilon_i = \sum_{j(\neq i)} (k_{ij} - 1)$ is the excess escape rate relative to the unit-rate reference. However, these

raw observables have undesirable redundancies. Conservation laws—time additivity $\sum_i T_i = t$ and Kirchoff's current balance $\sum_{j(\neq i)} N_{ij} \sim \sum_{j(\neq i)} N_{ji}$ [28]—enforce strong coupling among them in the long term, rendering the naive counts (N_{ij}, T_i) degenerate axes for control.

CFT resolves this redundancy by identifying the *asymptotically orthogonal* counting variables \mathbf{X} and relating the path entropy with their conjugate forces \mathfrak{F} —defined as the path entropy derivatives [26, 27]:

$$\ln \frac{\mathcal{P}_{\mathbf{k}}(\omega_t)}{\mathcal{P}_{\mathbf{u}}(\omega_t)} \sim \mathfrak{F}(\mathbf{k}) \cdot \mathbf{X}(\omega_t) - \mathfrak{c}(\mathbf{k}) t \quad (2)$$

where the caliber $\mathfrak{c}(t)$ resembles for our NEQ processes the role that the free energy plays for EQ processes. The vector $\mathbf{X} = (\Phi_{ij}, T_n, \Psi_c)$ is a complete observable basis consistent with the asymptotic constraints: (i) **edge traffic** $\Phi_{ij} = N_{ij} + N_{ji}$; (ii) **dwelt times** T_n (excluding a reference m); and (iii) **cycle net fluxes** $\Psi_c = N_{ab} - N_{ba}$, defined by the net flux across the chord ab of a fundamental cycle c (mnemonic: the time irreversible counterpart to traffic, $\Psi \equiv \text{“i”} + \Phi$). Dividing by time gives their rates $\mathbf{x} = (\phi_{ij}, f_n, \psi_c)$, and taking steady-state averages yields the intensive rate coordinate for the parameter space $\langle \mathbf{x} \rangle = \langle \mathbf{X} \rangle / t = (\tau_{ij}, \pi_n, J_c)$. Their conjugate forces \mathfrak{F} are the affinities to edge exchange, node dwelling, and cycle completion [26]:

$$\begin{aligned} \mathfrak{F}_{\text{edge}, ij} &= \frac{1}{2} \ln k_{ij} k_{ji}, \\ \mathfrak{F}_{\text{node}, n} &= \sum_{i(\neq n)} (k_{mi} - 1) - \sum_{j(\neq n)} (k_{nj} - 1), \\ \mathfrak{F}_{\text{cycle}, c} &= \frac{1}{2} \ln \frac{k_{i_0 i_1} k_{i_1 i_2} \cdots k_{i_{\sigma} i_0}}{k_{i_0 i_{\sigma}} k_{i_{\sigma} i_{\sigma-1}} \cdots k_{i_1 i_0}} \end{aligned} \quad (3)$$

where $i_0 i_1 i_2 \dots i_{\sigma} i_0$ is the state sequence of the cycle c . Crucially, the caliber rate $\mathfrak{c}(\mathbf{k}) = \sum_{j \neq m} (k_{mj} - 1)$ functions as the log dynamic partition function that generates observable statistics when parameterized by the forces \mathfrak{F} [26, 27].

The asymptotic form of Eq. (2) establishes fundamental *conjugate relations* between the observables and the forces. This conjugate structure dictates a fundamental duality between *observable fluctuations* and their corresponding *force responses*: the average susceptibility of the CFT rate observables x_{α} to a force \mathfrak{F}_{β} —while holding all other forces fixed—is exactly the asymptotic covariance [26]:

$$\left. \frac{\partial \langle x_{\alpha} \rangle}{\partial \mathfrak{F}_{\beta}} \right|_{\mathfrak{F}_{\gamma \neq \beta}} = \frac{\partial^2 \mathfrak{c}(\mathfrak{F})}{\partial \mathfrak{F}_{\alpha} \partial \mathfrak{F}_{\beta}} = \lim_{t \rightarrow \infty} t \text{Cov}[x_{\alpha}, x_{\beta}]. \quad (4)$$

Thus, fluctuations equal susceptibilities: (a) the strictly positive variance implies *monotonic* force responses: just as heat capacity is positive, any average rate observable $\langle x_{\alpha} \rangle \in (\tau_{ij}, \pi_n, J_c)$ must increase with its own conjugate drive \mathfrak{F}_{α} ; (b) the symmetry of covariance enforces a *generalized Maxwell-Onsager reciprocity* far from equilibrium: the

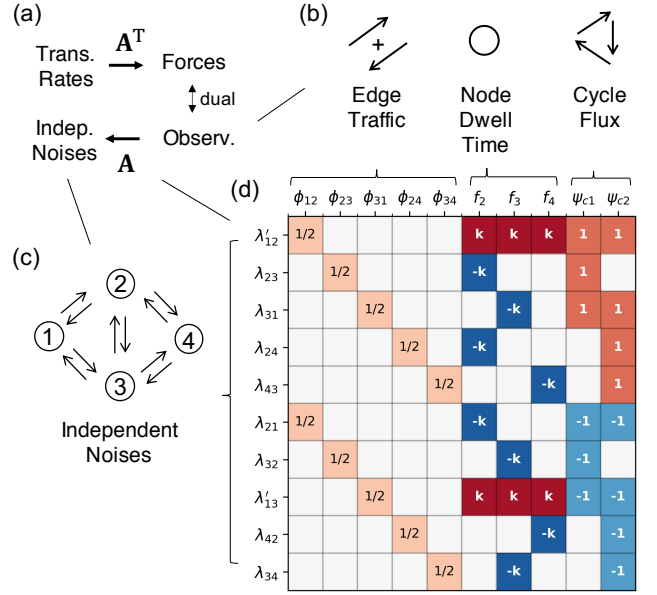


Figure 1. **The sparse structure of fluctuation-response duality.** (a) The Jacobian matrix \mathbf{A} acts as the bridge between stochasticity and control: it maps physical observables \mathbf{x} to independent noise sources λ (Fluctuation Geometry), while simultaneously linking transition rates $\ln \mathbf{k}$ to conjugate forces \mathfrak{F} (Response Geometry). (b) The complete observable basis: edge traffic ϕ_{ij} , node frequency f_n , and cycle net flux ψ_c . (c) A representative 4-state network showing that every transition edge generates an intrinsic independent noise source λ_{ij} . (d) The explicit structure of the Jacobian \mathbf{A} for the 4-state example. The symbol k (or $-k$) denotes the transition rate k_{ij} corresponding to the specific row index. The prime notation λ'_{mj} denotes the shifted noise source $\lambda'_{mj} = \lambda_{mj} + k_{mj}$ for transitions leaving the reference state $m = 1$. White squares denote structural zeros.

susceptibility of observable $\langle x_{\alpha} \rangle$ to force \mathfrak{F}_{β} is identical to the response of $\langle x_{\beta} \rangle$ to force \mathfrak{F}_{α} .

While the forces \mathfrak{F} have clear physical meanings as affinities, practical control more often involves tuning specific transition rates k_{ij} while fixing others, rather than manipulating one force while clamping the rest. We thus map the force-response conjugacy in CFT to the rate-response landscape:

$$\left. \frac{\partial \langle \mathbf{x} \rangle}{\partial \ln k_{ij}} \right|_{k_{ab}, ab \neq ij} = \sum_{\beta} \frac{\partial \langle \mathbf{x} \rangle}{\partial \mathfrak{F}_{\beta}} \frac{\partial \mathfrak{F}_{\beta}}{\partial \ln k_{ij}} \quad (5)$$

The projection is encoded by a sparse matrix $\mathbf{A}_{(ij), \beta} \equiv \partial \mathfrak{F}_{\beta} / \partial \ln k_{ij}$, the Jacobian linking the transition rates \mathbf{k} to the forces \mathfrak{F} [27], illustrated in Fig. 1.

To further operationalize this, we identify the independent noise sources, $\lambda_{ij} = (N_{ij} - k_{ij} T_i) / t$, in a Markov jump process, whose asymptotic covariances are diagonal [19]:

$$t \cdot \text{Cov}[\lambda_{ij}, \lambda_{mn}] \sim \pi_i k_{ij} \delta_{i,m} \delta_{j,n}. \quad (6)$$

These noise sources are asymptotically linearly spanned by

the CFT observables via the same Jacobian \mathbf{A} [27]:

$$\lambda[\omega_t] \sim \mathbf{A}(\mathbf{k}) \mathbf{x}[\omega_t] - \nabla_{\ln \mathbf{k}} c(\mathbf{k}). \quad (7)$$

Combining these yields the central **Response-Inverse-Matrix (RIM)** relation [27]:

$$\begin{aligned} \frac{\partial \langle x_\alpha \rangle}{\partial \ln k_{ij}} &= \lim_{t \rightarrow \infty} t \cdot \text{Cov}[x_\alpha, \lambda_{ij}] \\ &= \pi_i k_{ij} [\mathbf{A}^{-1}]_{\alpha, (ij)} \end{aligned} \quad (8)$$

where $\mathbf{A}^{-1} = \nabla_{\mathfrak{F}} \ln \mathbf{k}(\mathfrak{F})$ is the Jacobian from the forces to the transition rates.

These equations constitute a *fluctuation-response duality* for rate perturbations, originating from the underlying *observable-force conjugacy*: the Jacobian \mathbf{A} maps the CFT conjugates $(\mathbf{x}, \mathfrak{F})$ onto the kinetic variables $(\lambda, \ln \mathbf{k})$. While the first equality in Eq. (8) recovers a known result recently highlighted by Zheng and Lu [19], the second equality reveals the underlying dual geometry, identifying responses explicitly as matrix elements of the inverse Jacobian \mathbf{A}^{-1} . This gives three results: the linear mapping enables parsing fluctuations into independent components (Result 1); an algebraic closure of derivatives enables scalable gradient evaluation (Result 2); and Jacobian symmetries yield unified response relations, generalizing recent results [17, 18, 20] (Result 3).

Fluctuation–Response Relations are the key to design and optimization. While the statistical independence of noise sources λ is established [19], it is the linear mapping in Eq. (7) that identifies them as the complete, projectable coordinate axes. We exploit this geometric structure to decompose the total covariance between any two observables $x, x' \in (\phi_{ij}, f_n, \psi_c)$ into a sum over their projections onto the orthonormal axes:

$$\text{Cov}(x, x') \sim \sum_{i,j} \text{Cov}[x, \hat{\lambda}_{ij}] \cdot \text{Cov}[x', \hat{\lambda}_{ij}], \quad (9)$$

where $\hat{\lambda}_{ij} = \lambda_{ij} / \sqrt{\pi_i k_{ij} / t}$ is the unit-variance noise source at transition $i \mapsto j$. Geometrically, this is the inner product projection rule for vectors: $\mathbf{u} \cdot \mathbf{v} = \sum_z (\mathbf{u} \cdot \hat{\mathbf{e}}_z)(\mathbf{v} \cdot \hat{\mathbf{e}}_z)$. Crucially, the RIM relation (Eq. 8) further operationalizes this geometry. It transforms the covariance projections—which are otherwise difficult to derive from \mathbf{k} —into simple matrix elements. Every term in the decomposition becomes explicitly evaluable via the inverse Jacobian \mathbf{A}^{-1} .

We now apply Eq. (9) to a simple model of the kinesin molecular motor to illustrate how the motor “wastes time” through structural imprecision. We define a randomness parameter r : it is the variance-to-mean ratio of the net mechanical flux $\psi = (N_+ - N_-)/t$, where N_\pm denotes the forward and backward mechanical step counts. We express the motor’s

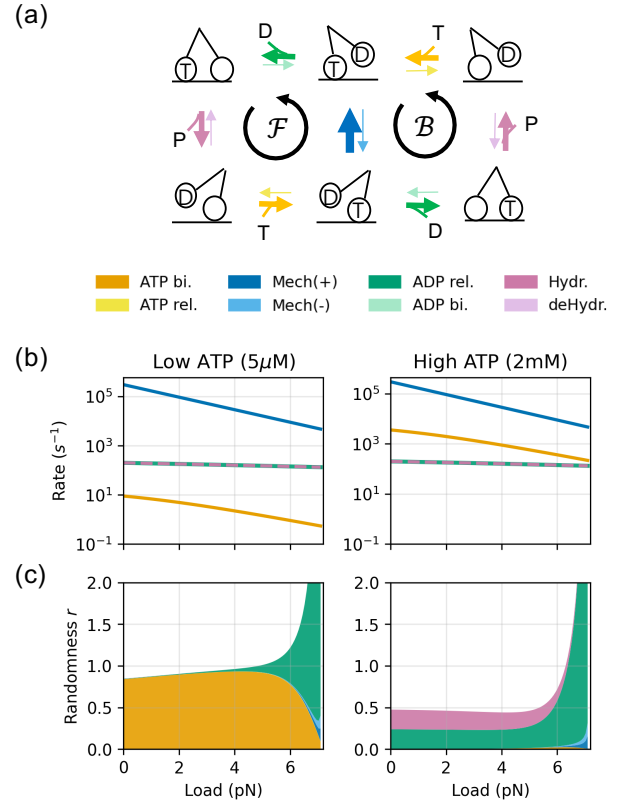


Figure 2. Dissecting Molecular Motor’s Randomness. (a) The 6-state model for kinesin [2]. (b) The bigger the load that the motor has to pull, the slower it runs, for given ATP energy sources [2]. (c) Decomposition of the motor’s randomness parameter r . The total randomness is decomposed into contributions from functional groups (aggregating forward \mathcal{F} and backward \mathcal{B} cycles), represented by the stacked areas. The upper boundary of the stacked areas is the randomness calculated by the kinesin model, fitted to Visscher et al. [29]. The motor becomes very inefficient when pulling heavy loads.

randomness in terms of its susceptibility:

$$\begin{aligned} r &= \lim_{t \rightarrow \infty} \frac{t \cdot \text{Var}(\psi)}{\langle \psi \rangle} = \lim_{t \rightarrow \infty} \frac{1}{\langle \psi \rangle} \sum_{i,j} \left(\text{Cov}[\psi, \hat{\lambda}_{ij}] \right)^2 \\ &= \frac{1}{\langle \psi \rangle} \sum_{i,j} \underbrace{\frac{k_{ij}}{\pi_i} \left(\frac{\partial \langle \psi \rangle}{\partial k_{ij}} \right)^2}_{\text{Sensitivity Contribution}}. \end{aligned} \quad (10)$$

This shows that imprecision couples to responsiveness: since the noise contribution scales with the squared sensitivity $(\partial \langle \psi \rangle / \partial k)^2$, a highly responsive step “amplifies” its own intrinsic noise into the overall variance. Crucially, this result moves beyond bounds like thermodynamic uncertainty relations [25, 30, 31] which constrain the *magnitude* of flux randomness based on global dynamical time irreversibility. Instead, Eq. (10) provides an *exact mechanistic decomposition* in terms of kinetic covariances and sensitivities. This approach directly identifies which specific molecular transitions act as the primary sources of the motor’s randomness,

enabling the targeted dissection of the motor’s stochastic mechanism shown below.

The power of Eq. (10) is illustrated by a new insight it gives into the molecular bases for the motor’s behavior. Fig. 2(b-c) reveals a shift in the stochasticity mechanism of kinesin: (i) For small loads (far from stalling), the motor is dominated by the *timing noise*, arising from the rate-limiting forward step(s)—the arrival of ATP at low [ATP] or the ADP release and ATP hydrolysis at high [ATP]. (ii) For big loads (near the stall force, green region), fluctuations are dominated by a *branching noise*. That is, near stall, the backward mechanical rate becomes comparable to the forward rate, and the ADP release step dominates the randomness because it controls the critical partitioning between the forward and backward cycles. This transition in fluctuation properties—between waiting for steps and committing to a step—is not obtainable from approaches that only analyze mean rates; it requires the fluctuation-response relations here.

The CFT formalism enables scalable design. To optimize the randomness parameter r by varying transition rate parameters k_{ij} , for example using zero-gradient conditions ($\nabla_k r = 0$) or by driving iterative gradient descent, the computational bottleneck entails evaluating the full gradient of r with respect to all rate constants. While analytical expressions for this exist, this evaluation becomes computationally prohibitive for large-scale models. Standard numerical approaches based on generating functions, such as finite differences combined with eigenvalue solvers (e.g., Koza’s method [24, 25]), are costly because they require recomputing the function for every parameter perturbation.

Here, we show that our \mathbf{A}^{-1} formalism breaks this bottleneck by ensuring algebraic closure: the gradient of the inverse matrix is fully determined by the inverse itself ($\partial \mathbf{A}^{-1} = -\mathbf{A}^{-1}(\partial \mathbf{A})\mathbf{A}^{-1}$). This allows evaluating both the gradients of mean and variance with a single inverse matrix, significantly improving scalability for locally connected networks—those with $N_{\text{edge}} = \mathcal{O}(N_{\text{node}})$, typical in biophysical models.

Again for illustration, we use the kinesin model. To capture the continuous diffusive nature of the mechanical swing, we extend the single-hop transition in Liepelt and Lipowsky’s model [2] into a biased random walk across N substeps on a lattice (Fig. 3a). We take the chemical rates directly from their original model [27]. We benchmarked both methods by computing the full gradient under different numbers of mechanical substeps. As shown in Fig. 3(b), the brute-force method (red) scales as $\mathcal{O}(N^{3.1})$. In contrast, our \mathbf{A}^{-1} approach (blue) scales better, as $\mathcal{O}(N^{1.6})$, yielding a >100 -fold speed-up for networks with $N_{\text{node}} \approx 100$. While our edge-centric algorithm theoretically scales less favorably for dense graphs ($N_{\text{edge}} = \mathcal{O}(N_{\text{node}}^2)$), we show in the Supplemental Material [27] that it remains computationally

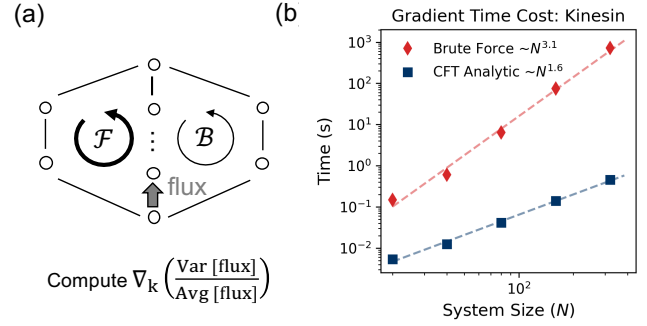


Figure 3. **Breaking the Computational Bottleneck.** (a) The Θ -shape topology used for benchmarking, representing a generalized motor model with multiple mechanical substeps to mimic the diffusive stepping process. (b) Scaling of the computation time for the gradient of the randomness parameter (ratio of variance and average of the flux) as a function of the number of mechanical substeps (and thus the system size).

superior even on fully connected networks with sizes up to $N_{\text{node}} \approx 100$.

Universal symmetries and kinetic bounds. The geometric structure of the Jacobian \mathbf{A} dictates universal principles that govern how any steady-state observables respond to perturbations in any ergodic network flow. From the identity $\mathbf{A}^{-1}\mathbf{A} = \mathbf{I}$, we derive three sets of local response symmetries [27], valid for arbitrary CFT observables $\langle x \rangle \in \{\pi_n, \tau_{ij}, J_c\}$. This unifies and generalizes existing response relations [17, 20] within a single principle-based framework.

On each node n , we derive a **Node Escaping Symmetry**:

$$\sum_{l(\neq m)} \frac{k_{ml}}{\pi_m} \frac{\partial \langle x \rangle}{\partial k_{ml}} - \sum_{j(\neq n)} \frac{k_{nj}}{\pi_n} \frac{\partial \langle x \rangle}{\partial k_{nj}} = \delta_{\langle x \rangle, \pi_n} \quad (11)$$

where the right-hand side is a Kronecker delta, introducing an additional factor of 1 only if $\langle x \rangle = \pi_n$. This generalizes the response equalities derived by Owen *et al.* [17] from state probabilities to arbitrary CFT observables. On each edge ij , we have an **Edge Reciprocity**:

$$\frac{1}{\pi_i} \frac{\partial \langle x \rangle}{\partial k_{ij}} + \frac{1}{\pi_j} \frac{\partial \langle x \rangle}{\partial k_{ji}} = 2\delta_{\langle x \rangle, \tau_{ij}}. \quad (12)$$

Together with our covariance decomposition in Eq. (9), they underpin the flux fluctuation-response identities derived by Aslyamov *et al.* [20], while extending their validity to arbitrary CFT observables. On each cycle c , we find a **Cycle Symmetry**:

$$\sum_{ij \in c^+} \frac{1}{\pi_i} \frac{\partial \langle x \rangle}{\partial k_{ij}} - \sum_{ji \in c^-} \frac{1}{\pi_j} \frac{\partial \langle x \rangle}{\partial k_{ji}} = 2\delta_{\langle x \rangle, J_c}. \quad (13)$$

This enforces a topological constraint: the cumulative sensitivity along any forward cycle must precisely balance

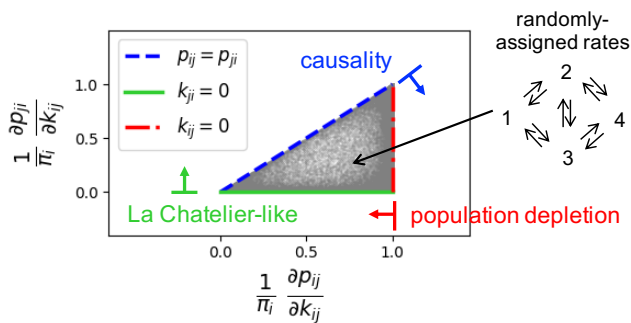


Figure 4. **Universal Kinetic Bounds.** The scatter plot numerically validates the derived sensitivity hierarchy using an ensemble of random 4-state networks as an example (schematic, upper right). Each grey dot represents the normalized response of the forward flux p_{ij} (x-axis) versus the induced response of the reverse flux p_{ji} (y-axis) to a perturbation in the forward rate k_{ij} . The feasible response region is strictly bounded by three physical limits: Population Depletion, Causality, and Le Chatelier-like Compensation.

that of its reversal (for observables $\langle x \rangle \neq J_c$). See [27] for derivation details and correspondences to past results.

Our framework also provides the physical origins of established response bounds. By identifying the algebraic coefficients Δ_{ij} and ∇_{ij} appeared in Aslyamov and Esposito [18] as specific rate sensitivities [27]:

$$\pi_i(1 - \Delta_{ij}) = \frac{\partial J_{ij}}{\partial k_{ij}} \quad \text{and} \quad \pi_i(1 + \nabla_{ij}) = \frac{\partial \tau_{ij}}{\partial k_{ij}}, \quad (14)$$

we elevate their algebraic constraints ($0 \leq \Delta_{ij} \leq 1$ and $|\nabla_{ij}| \leq \Delta_{ij}$) into a physical kinetic hierarchy for the one-way fluxes $p_{ij} = \pi_i k_{ij}$:

$$\pi_i \geq \frac{\partial p_{ij}}{\partial k_{ij}} \geq \frac{\partial p_{ji}}{\partial k_{ij}} \geq 0. \quad (15)$$

As visualized in the triangular domain of Fig. 4, this hierarchy reflects the physical mechanisms governing nonequilibrium flow response, valid for any steady-state network flows.

The upper bound, $\pi_i \geq \partial_{k_{ij}} p_{ij} = \pi_i + k_{ij} \partial_{k_{ij}} \pi_i$, reflects *population depletion*: since increasing the escape rate k_{ij} drains the source population ($\partial_{k_{ij}} \pi_i \leq 0$), the flux cannot grow faster than the population size π_i . This limit is saturated as $k_{ij} \rightarrow 0$, where the perturbation is too weak to shift the steady-state population. The middle inequality, $\partial_{k_{ij}} p_{ij} \geq \partial_{k_{ij}} p_{ji}$, reflects *causality* ($\partial_{k_{ij}} J_{ij} \geq 0$), showing a stronger push always increases net flux in the driven direction. This bound tightens to equality ($p_{ij} = p_{ji}$) at zero-flux edges, characteristic of detailed balance or a topological bridge. Finally, the non-negativity of the induced reversed response ($\partial_{k_{ij}} p_{ji} \geq 0$) captures a *Le Chatelier-like compensation*: pushing “particles” into the target state j increases its occupancy, which in turn drives an increased

reverse backflow even when the reverse rate k_{ji} remains fixed.

Conclusions: We have presented a force-based framework for nonequilibrium fluctuations and responses. It bridges between formal variational theory and computational utility. These relations reflect a deeper observable-force conjugacy, encoded in the inverse of a single Jacobian matrix. We demonstrated its dual utility: Analytically, it reveals principles of design and optimization, as shown in the kinesin molecular motor. Computationally, it scales efficiently for large networks. And it reveals general response relations and universal constraints on stochastic flows.

Code Availability: The code used to produce the Figures are available at <https://doi.org/10.5281/zenodo.18611573>.

Acknowledgments: We are grateful for financial support from the Laufer Center for Physical and Quantitative Biology at Stony Brook, the John Templeton Foundation (Grant ID 62564), and NIH (Grant RM1-GM135136).

* ying-jen.yang@stonybrook.edu

- [1] A. B. Kolomeisky and M. E. Fisher, Molecular Motors: A Theorist’s Perspective, *Annual Review of Physical Chemistry* **58**, 675 (2007), [_eprint: https://doi.org/10.1146/annurev.physchem.58.032806.104532](https://doi.org/10.1146/annurev.physchem.58.032806.104532).
- [2] S. Liepelt and R. Lipowsky, Kinesin’s Network of Chemomechanical Motor Cycles, *Phys. Rev. Lett.* **98**, 258102 (2007).
- [3] J. A. Wagoner and K. A. Dill, Mechanisms for achieving high speed and efficiency in biomolecular machines, *PNAS* **116**, 5902 (2019).
- [4] T. A. J. Duke, N. Le Novère, and D. Bray, Conformational spread in a ring of proteins: a stochastic approach to allostery I, *Journal of Molecular Biology* **308**, 541 (2001).
- [5] Y. Tu, The nonequilibrium mechanism for ultrasensitivity in a biological switch: Sensing by Maxwell’s demons, *Proceedings of the National Academy of Sciences* **105**, 11737 (2008).
- [6] J. Monod, J. Wyman, and J.-P. Changeux, On the nature of allosteric transitions: A plausible model, *Journal of Molecular Biology* **12**, 88 (1965).
- [7] J. J. Hopfield, Kinetic Proofreading: A New Mechanism for Reducing Errors in Biosynthetic Processes Requiring High Specificity, *PNAS* **71**, 4135 (1974).
- [8] J. Ninio, Kinetic amplification of enzyme discrimination, *Biochimie* **57**, 587 (1975).
- [9] H. Qian and E. L. Elson, Single-molecule enzymology: stochastic Michaelis–Menten kinetics, *Biophysical Chemistry Special issue in honour of John A Schellman*, **101-102**, 565 (2002).
- [10] A. Goldbeter and D. E. Koshland, An amplified sensitivity arising from covalent modification in biological systems., *Proceedings of the National Academy of Sciences* **78**, 6840 (1981).
- [11] H. Qian, Phosphorylation Energy Hypothesis: Open Chemical Systems and Their Biological Functions, *Annual Review of Physical Chemistry* **58**, 113 (2007).
- [12] T. L. Hill, *Free Energy Transduction and Biochemical Cycle Kinetics* (New York, 1989).
- [13] A. I. Brown and D. A. Sivak, Theory of Nonequilibrium Free

- Energy Transduction by Molecular Machines, *Chem. Rev.* **120**, 434 (2020).
- [14] J. Schnakenberg, Network theory of microscopic and macroscopic behavior of master equation systems, *Rev. Mod. Phys.* **48**, 571 (1976).
- [15] M. Baiesi, C. Maes, and B. Wynants, Fluctuations and Response of Nonequilibrium States, *Phys. Rev. Lett.* **103**, 010602 (2009).
- [16] U. Seifert and T. Speck, Fluctuation-dissipation theorem in nonequilibrium steady states, *EPL* **89**, 10007 (2010).
- [17] J. A. Owen, T. R. Gingrich, and J. M. Horowitz, Universal Thermodynamic Bounds on Nonequilibrium Response with Biochemical Applications, *Phys. Rev. X* **10**, 011066 (2020).
- [18] T. Aslyamov and M. Esposito, Nonequilibrium Response for Markov Jump Processes: Exact Results and Tight Bounds, *Phys. Rev. Lett.* **132**, 037101 (2024).
- [19] J. Zheng and Z. Lu, *Nonlinear Response Relations and Fluctuation-Response Inequalities for Nonequilibrium Stochastic Systems* (2025), arXiv:2509.19606 [cond-mat].
- [20] T. Aslyamov, K. Ptaszyński, and M. Esposito, Nonequilibrium Fluctuation-Response Relations: From Identities to Bounds, *Phys. Rev. Lett.* **134**, 157101 (2025).
- [21] G. Fernandes Martins and J. M. Horowitz, Topologically constrained fluctuations and thermodynamics regulate nonequilibrium response, *Phys. Rev. E* **108**, 044113 (2023).
- [22] J. A. Owen and J. M. Horowitz, Size limits the sensitivity of kinetic schemes, *Nat Commun* **14**, 1280 (2023).
- [23] K. Ptaszyński, T. Aslyamov, and M. Esposito, Dissipation Bounds Precision of Current Response to Kinetic Perturbations, *Phys. Rev. Lett.* **133**, 227101 (2024).
- [24] Z. Koza, General technique of calculating the drift velocity and diffusion coefficient in arbitrary periodic systems, *J. Phys. A: Math. Gen.* **32**, 7637 (1999).
- [25] A. C. Barato and U. Seifert, Thermodynamic Uncertainty Relation for Biomolecular Processes, *Phys. Rev. Lett.* **114**, 158101 (2015).
- [26] Y.-J. Yang and K. A. Dill, *A Principled Basis for Nonequilibrium Network Flows* (2025), arXiv:2410.17495v3 [cond-mat].
- [27] See Supplemental Material at [URL] for more details.
- [28] We use standard asymptotic analysis notation $a \sim b$ to represent asymptotic equivalency, $\lim_{t \rightarrow \infty} a(t)/b(t) = 1$.
- [29] K. Visscher, M. J. Schnitzer, and S. M. Block, Single kinesin molecules studied with a molecular force clamp, *Nature* **400**, 184 (1999).
- [30] T. R. Gingrich, J. M. Horowitz, N. Perunov, and J. L. England, Dissipation Bounds All Steady-State Current Fluctuations, *Phys. Rev. Lett.* **116**, 120601 (2016).
- [31] J. M. Horowitz and T. R. Gingrich, Thermodynamic uncertainty relations constrain non-equilibrium fluctuations, *Nat Phys* **16**, 15 (2020).